DOI: 10.1002/ ((please add manuscript number))
Article type: Full Paper

Monothiatruxene based solution-processed green, sky-blue and deep-blue organic light-emitting diodes with efficiencies beyond 5% limit

Michal R. Maciejczyk, Shuyu Zhang[1], Gordon J. Hedley[2], Neil Robertson*, Ifor D. W. Samuel,* and Marek Pietraszkiewicz*

Dr. M. R. Maciejczyk, Prof. M. Pietraszkiewicz
Institute of Physical Chemistry, Polish Academy of Sciences,
Kasprzaka 44/52, Warsaw, 01-224, Poland
E-mail: m.maciejczyk@ed.ac.uk

Dr. S. Zhang, Dr. G. J. Hedley, Prof. I. D. W. Samuel
Organic Semiconductor Centre, SUPA, School of Physics and Astronomy, University of St. Andrews, North Haugh, St. Andrews, Fife, KY16 9SS, UK.
E-mail: idws@st-andrews. ac.uk

Prof. N. Robertson, Dr. M. R. Maciejczyk
EaStCHEM School of Chemistry, University of Edinburgh,
King's Buildings, Edinburgh EH9 3FJ, UK
E-mail: neil.robertson@ed.ac.uk

Keywords: organic light-emitting diodes (OLEDs), blue emitters, solution-processed, truxenes, donor-acceptor

The development of blue materials with good efficiency, even at high brightness, with excellent color purity, simple processing and high thermal stability assuring adequate device lifetime is an important remaining challenge for organic light-emitting didoes (OLEDs) in displays and lightning applications. Furthermore, these various features are typically mutually exclusive in practice. Herein, four novel green and blue light emitting materials based on a monothiatruxene core are reported together with their photophysical and thermal properties, and performance in solution-processed OLEDs. The materials showed excellent thermal properties with high glass transition temperatures ranging from 171 °C to 336 °C and decomposition temperatures from 352 °C to 442 °C. High external quantum efficiency of 3.7 % for a deep blue emitter with C.I.E. color co-ordinates (0.16, 0.09) and 7% for green

[1] Department of Light Sources and Illuminating Engineering, Fudan University, Shanghai 200433, People's Republic of China; Engineering Research Center of Advanced Lighting Technology, Ministry of Education, and Institute of Beyond Lighting, Academy for Engineering and Technology, Fudan University, Shanghai 200433, People's Republic of China.
[2] School of Chemistry, University of Glasgow, Joseph Black Building, University Avenue, Glasgow, G12 8QQ, UK.

emitter with color co-ordinates (0.22, 0.40) was achieved at 100 cd/m^2. The efficiency observed was exceptionally high for fluorescent materials with a photoluminescence quantum yield of 24 % and 62%, respectively. The performance at higher brightness was very good with only 38% and 17% efficiency roll-off at 1000 cd/m^2. The results indicate that utilization of this unique molecular design is promising for efficient deep blue highly stable and soluble light-emitting materials.

1. Introduction

Advanced organic materials for organic electronics and photonics have been of particular interest in the past decade. Highly photoluminescent compounds have found numerous applications in fluorescent sensors,[1–5] biomarkers,[6–9] organic light-emitting diodes (OLEDs),[10–15] and organic photovoltaics (OPV).[16–20] Particular emphasis has been placed on OLED and OPV technologies as a means to solve world energy problems, by enabling energy-saving light sources, and sustainable electric energy from the sun. OLED technology is particularly interesting for its potential to be used both for solid-state lighting, and in numerous display applications. The evolution of key emissive components in this respect has evolved from fluorescent materials[21] to platinum group phosphorescent emitters based on cyclometallated heterocyclic compounds,[22–24] to more recently, single-molecule emitters based on triplet-triplet annihilation (TTA),[25–28] thermally activated delayed fluorescence (TADF),[29–40] hybridized local and charge-transfer excited states (HLCT),[41] and horizontally-oriented materials.[42–46] According to spin statistics, charges injected into OLED active layers recombine to give 75 % triplets and 25 % singlets. This imposes a severe limitation on fluorescent emitters because in traditional fluorescent organic materials only singlet excitons lead to radiative decay and then generate light. This gives four times lower efficiency than noble-metal-based devices since higher efficiency is achieved with

phosphorescent iridium-based metallacycle emitters in which strong spin-orbit coupling of the heavy-metal center enhances intersystem crossing. However, the high price of platinum metals, lack of stable long-lifetime blue emitting phosphors, and lower electroluminescence efficiency under high current densities,[47,48] call for alternative solutions. Solution-processing is desirable for large area coating and brings additional materials requirements such as high solubility, which can be problem for some metal complexes in organic solvents.[49] These concerns hinder OLED technology from realizing its full potential for cheap lighting and large screen display applications.

The recent development of organic materials that display TADF and TTA phenomena have shown that even pure organic compounds can harvest both singlets and triplets to give highly efficient OLEDs. In the TADF approach, a small energy gap between the triplet and singlet allows Reverse Intersystem Crossing (RISC) from the first excited triplet state (T_1) into the first excited singlet state (S_1) which can be achieved by spatial separation of the donor and acceptor parts of molecules to give a singlet-triplet gap small in comparison to thermal energy. Additionally, the efficiency of light extraction in OLEDs is typically in the region of 20-30 %,[50] so even devices with high internal quantum efficiency (IQE) are limited by this factor. Light extraction can be increased by attaching scattering refracting or diffracting light structures outside or inside of the device.[51] Moreover, careful design of the emitting molecules leading to horizontal orientation of the light-emitting transition dipoles can enhance light outcoupling efficiency and give values of the external quantum efficiency (EQE) as high as 35% (device based on iridium complex).[52]

Our research interest in truxenes and heterotruxenes has prompted us to investigate these in the context of the TADF-emitters and horizontally-oriented materials fields. Recent utilization of horizontally oriented TADF emitters demonstrated extremely high EQEs at the level of 37% for sky-blue,[53] and 29% for orange-red.[54]. Truxene and triheterotruxenes are well known discotic liquid crystal materials,[55–57] and so are excellent candidates to realise

horizontal orientation. Furthermore they are known to have excellent thermal and photochemical stability,[58] for instance, bare monosulfonyltruxene core ($TrxSO_2$) presented here has glass transition temperature of 119 ºC, melting point of 256 ºC and decomposes at 357 ºC.[59] It is conceivable that appropriate functionalisation by donor and acceptor groups could additionally make them TADF emitters as has been very recently reported by utilization of triazatruxene substituted with three peripheral acceptors leading to green organic light-emitting diode devices with external quantum efficiency over 30% at 76 cd/cm^2.[60]

Truxene possesses a C_3-symmetrical heptacyclic π-conjugated central core and was used as a material for two-photon absorption[61], OLEDs,[62–64] organic field effects transistors,[65] dye-sensitized solar cells,[66] organic lasers[67] and fluorescent probes.[68,69]. We have recently reported the first synthesis of monothiatruxenes,[59] merging two classes of molecules, truxene and trithiatruxene, to provide a platform for diverse structural modification. This has been followed by introducing other heteroatoms to truxene core like oxygen, leading to oxatruxene, a molecule with enhanced fluorescence quantum yield in comparison to its all-carbon counterpart by factor of 4.[70]

Bright blue light-emitting materials for application in displays are of high demand but they need to meet certain criteria of color purity: Commission Internationale de L'Eclairage coordinates (CIE x, y) of (0.14, 0.08) are required by the National Television System Committee (NTSC) while High-Definition Television (HDTV) ITU-R BT.709 requires a deeper blue emission with CIE x, y of (0.15, 0.06). Typically, in the literature the deep blue emission is defined as having a CIE coordinates $y < 0.15$ and $x + y < 0.30$.[71] In the review from 2017[72] "the bluest" TADF emitter with CIE coordinates (0.15, 0.07) obtained efficiency of 9.9 % but at 0.1 cd/m^2, very low impractical luminance. At higher brightness of 300 cd/m^2 the EQE dropped below 1%.[73] This is a typical behaviour of deep blue emitters as it is difficult to design material that will simultaneously inject electrons and holes into such wide band-gap organic semiconductor as the deep color of emission is obtained by restricting

the π-conjugation length, therefore inhibiting carrier injection and transport.[74] State of the art OLED materials with CIE coordinates close to above values namely: x≤0.16 and y≤0.10, are depicted in **Table 1**. Common structural feature is that 4 of them have imidazole in their structure, 3 of them have phenanthroimidazole and another 3 have pyrene. This has been combined with different donor and acceptor substituents like: phosphine oxide, diphenyl amine, sulfone, thiazine and dimehtyldihydroacridine. Therefore, one can say that due to limitation impose on blue emitters there might be defined structural design of these materials narrowing their variety and introduction new approaches should be of high value. The highest efficiency achieved among presented emitters is up to 7.3 % at 500 cd/m^2 (CIE 0.14, 0.10) with typical value around 5%. These are much lower values then obtained for other types of OLED emitters, like sky-blue or green, highlighting difficulty in designing efficient material that will maintain high efficiency in a range 360 to 409 cd/m^2 (a minimum luminance of OLED display under 0 to 5000 lux conditions in order to reproduce high-image-quality).[75] Additionally, compounds with donor-acceptor structures suffer from great efficiency roll-off at higher brightness as presented in **Table 1** entries 4, 6 and 7. Limiting them to low light intensity applications. Therefore, there is necessity in introduction novel materials that will deliver deep blue emission in order to push efficiencies even higher. Truxene molecule seems to be very promising core in these terms which despite large condensed aromatic structure retains deep blue emission. At the same time exhibiting great charge transport properties to be recently called a “rising star” in the review on: *Truxene as a Promising Hole Transport Material in Perovskite Solar Cells*.[76]

In this work, we have studied new monothiatruxene derivatives as green, sky-blue and deep-blue emitting materials, possessing high thermal stability and solubility for spin-coated[77] OLEDs, leading to external quantum efficiencies 2-3 times higher than those expected for fluorescent emitters with luminance as high as 10 000 cd/cm^2 and low efficiency roll-off. Although very high efficiencies have been reported for green and sky blue, deep blue

materials are typically only a few percent efficient. Efficiencies presented here for non-optimized deep blue devices with CIE coordinates close to NTSC and HDTV standards are very promising reaching up to 3.9 % with very low efficiency roll-off at 1000 cd/m^2 of only 38%. Largely exceeding typical values of efficiency roll-off at that high brightnesses for deep blue emitters based on donor-acceptor structure state-of-the-art materials as presented in Table 1. Additionally, studied compounds show high glass transition temperature from 171 ºC to 336 ºC, promising great device stability and long operation lifetime.

2. Results and Discussion

2.1. Synthesis

Novel target materials (**Scheme 1**) were synthesized from our previously reported di- and tri-brominated monothiatruxene[59] with solubilizing ethyl groups via Buchwald-Hartwig amination for carbazole (Cz) and dipehylamine (DPA) as substrates or Sonogashira coupling in the case where the reacting group was terminal alkyl. The yields of the reaction vary from very good 86% for Sonogashira coupling through good 72-73% for Buchwald-Hartwig di-amination to moderate 53% for tris-amination. The design of the final materials has been chosen to test the influence of the number of substituents and the π-spacer. Backbone acts as an electron acceptor and para or meta connected diphenylamine and carbazole serve as strong and weak donors, respectively. Introduction of weaker donor as carbazole in combination with sulfone unit should be especially interesting as has been previously shown that this type of structure makes deep blue emitters.[71] In 2ATPATrxSO_2, phenyl acetylene was introduced between truxene core and dipheylamine in order to increase the locally excited (LE) component by extending π-conjugation and increasing photoluminescence efficiency while keeping the same donor strength. The chemical structure and purity of the emitters was confirmed with ^{1}H and ^{13}C NMR, mass spectrometry, elemental analysis and X-ray crystallography. Full experimental details and characterization can be found in the supporting information.

2.2. X-ray crystallographic analysis

In order to gain further insights into these material the structure of 2CzTrxSO$_2$ has been studied by single-crystal X-ray diffraction (**Figure 1**). The data of X-ray analysis are summarized in Table S 3. The compound formed pale yellow crystals from dichloromethane/hexane solution crystallizing in triclinic space group P-1 along with one molecule of hexane. The asymmetric unit contains one fully ordered molecule of 2CzTrxSO$_2$ which was modelled as positionally-disordered about a crystallographic inversion centre. Due to the flat structure, π-π stacking is found with the distance of 3.77 Å and plane shift (i.e. lateral offset of the π-π stacking molecules) of 0.88 Å. This interaction is supported by formation of intermolecular C-H…O-S hydrogen bonds with length of 2.54 Å. Additionally intramolecular C-H…O-S hydrogen bonds are observed with 2.58 Å length. These findings are in agreement with the increased melting and decomposition temperatures from 208 ºC and 326 ºC for monothiatruxene to 256 ºC and 357 ºC for monosulfonyltruxene, as we previously reported.[59] Two different values of dihedral angles of 51º and 79º between carbazole substituents and truxene core were observed. Based on these results, this planar molecular structure should possess good stability under exciton formation and good thermal stability to provide long lifetime of the manufactured devices.

2.3. Thermal properties

To study the thermal properties of presented materials thermogravimetric analysis (TGA) and differential scanning calorimetry (DSC) were used, as shown in **Table 2** and Figures from S6 to S10 in ESI. Obtained values of glass transition temperatures can be explained by comparing molecular weight and symmetry of molecules. Therefore, the highest value of 336 ºC has been observed for the heaviest molecule 2ATPATrxSO$_2$, this should be followed by second heaviest molecule 3CzTrxSO$_2$ but due to unsymmetrical substitution of the third carbazole it has lower Tg than 2CzTrxSO$_2$. The very high glass transition temperatures are

desirable for OLEDs being the most important factor which affects device stability, because materials with low T_g can easily crystallize during driving operation, resulting in reduced device lifetime.[78,79] Therefore, presented approach show the advantage of using truxene to give branched structures to confer solubility. In contrast the commonly used strategy of using aliphatic side-chains to enhance solubility can lead to an undesirable lowering of glass transition temperature.[80] As expected the lowest value was observed for the material 2DPATrxSO2 with more elastic diphenylamine substituents. The same trend has been observed for decomposition temperatures ranging from 352 ºC for 2DPATrxSO_2 to 442 ºC for 2ATPATrxSO_2 with less than 20% mass loss for three of presented materials at temperature as high as 500 ºC. All the compounds exhibit excellent thermal properties and furthermore are readily solution processable to make good films.

2.4. Photophysical properties

The photophysical properties of materials were analysed by UV-vis and photoluminescence (PL) measurements. The absorption spectrum of thin films, photoluminescence spectra in toluene solution at room temperature and 77 K, neat thin films and doped in host material are displayed in **Figure 2**.

All compounds reveal a weak lowest-energy absorption band which can be attributed to the intramolecular charge-transfer (ICT). Compared with carbazole, absorption maximum λ_{abs}= 350 nm, the triphenylamine (λ_{abs}= 394 nm) and diphenylamine (λ_{abs}= 400 nm) modified structures exhibit a red shifted absorption in neat films, which can be attributed to the stronger electron donor ability of TPA and DPA.

The same trend is observed in the fluorescence spectra of degassed toluene solutions the emission maximum red shifts with the number of donor groups: 2Cz λ_{fl}= 430 nm, 3Cz λ_{fl}= 440 nm and donor strength 2TPA λ_{fl}= 450 nm, 2DPA λ_{fl} = 475 nm. On the other hand, in PL spectra of neat films the order is altered with λ_{fl}= 460 nm for 2Cz and 3Cz and redshifted

emission maximum for 2DPA (λ_{fl}= 510 nm) and 2TPA (λ_{fl}= 540 nm). For the doped films in 4,4'-bis(N-carbazolyl)-1,1'biphenyl (CBP) host with concentration of 7%, spectra are blue shifted, in comparison to neat films, by 22 nm for 3Cz, 30 nm for 2Cz, 35 nm for 2DPA and 40 nm for 2TPA. In general no significant difference, in terms of polarity and dilution influence, was observed upon adding an additional carbazole unit to $2TrxSO_2$. This can be explained by the *meta* position of the substitution preventing interaction with the truxene core. All fluorescence spectra are structureless, which can be attributed to intramolecular CT fluorescence. Therefore, the almost identical fluorescence wavelength shifts for three of the compounds in toluene solution and doped films might be explained by changing the polarity of the environment. Different behaviour was observed for the compound with phenyl acetylene spacer ($2ATPATrxSO_2$), since much stronger emission redshifting is observed going from solution through CBP matrix to neat films in the range of 50 nm each. The fluorescence quantum yield of $2ATPATrxSO_2$ ($\Phi_{sol/neat/host}$= 0.58/0.25/0.62) is the highest followed by $2DPATrxSO_2$ ($\Phi_{sol/neat/host}$= 0.20/0.19/0.37), $2CzTrxSO_2$ ($\Phi_{sol/neat/host}$= 0.25/0.17/0.24), $3CzTrxSO_2$ ($\Phi_{sol/neat/host}$= 0.21/0.14/0.20). As can be seen from these data the tris substituted derivative reveals a small drop of photoluminescence quantum yield of neat films. The strongest increase for $2ATPATrxSO_2$ after dilution in CBP host, indicates the presence of strong intermolecular interactions for this molecule. The triplet energy levels determined from the onset of phosphorescence bands in toluene solutions at 77 K were estimated to be at 2.30 eV, 2.37 eV, 2.52 eV and 2.54 eV for materials with diphenylamine with phenyl acetylene, diphenylamine, three carbazoles and two carbazoles as substituents, respectively. While singlet energy levels were determined from the maximum of the emission in deaerated toluene solution. In the present series, compounds $2DPATrxSO_2$ has the smallest ΔE_{ST} gap, around 0.24 eV, while compounds $2CzTrxSO_2$, $ATPATrxSO_2$ and $3CzTrxSO_2$ have larger gap from 0.34 eV, 0.46 eV and 0.30 eV, respectively. These energy differences are within the range of TADF (typically below 0.37 eV),[81] mechanism for three of the studied

compounds. Only 2ATPATrxSO$_2$ has energy gap higher than that required to realize TADF mechanism possible. Although, these determinations have been done for toluene solutions where 2ATPATrxSO$_2$ showed weak phosphorescence intensity with additional weak band at 2.64 eV, to give ΔE_{ST}= 0,12 eV, which has not be taken into consideration. Moreover, 2ATPATrxSO$_2$ showed the biggest polarity/dilution influence on the emission peak position, therefore TADF mechanism might be anticipated in this case as well. This has been supported by recording PLQY in aerated and degassed toluene solution where 2ATPATrxSO$_2$ showed the biggest increase, when degassed, from 58% to 62% while 2DPATrxSO$_2$ from 19% to 21%, while 2CzTrxSO$_2$ and 3CzTrxSO$_2$ showed no difference. Although, no long-lived emission was observed in degassed solutions as the lifetime of emission were around 2 ns for all the studied materials (see **Table 3**). To investigate this further, solid state measurements were done. Here, on other hand both 2CzTrxSO$_2$ and 3CzTrxSO$_2$ were found to have three components with the longest component of 15% and 7% contribution and 45 and 36 ns lifetime under vacuum for 3Cz and 2Cz derivative, respectively. While 2DPATrxSO$_2$ and 2ATPATrxSO$_2$ had only one delayed component with 10 ns and 8 ns lifetime, and 4% and 7% contribution, respectively. A summary of the photophysical data is presented in Table 1; for more detailed information see supporting information (SI). A summary of the photophysical data is presented in **Table 3**.

2.5 Electrochemical properties

Cyclic (CV) and square-wave voltammetry (SWV) was performed to investigate the electrochemical behaviour of the materials. All of the investigated compounds showed both oxidation and reduction processes. As shown in **Figure 3**, 3CzTrxSO$_2$ and 2DPATrxSO$_2$ display two oxidation processes while 2CzTrxSO$_2$ and 2ATPATrxSO$_2$ display only one. The lowest oxidation potential is observed for diphenylamine substituted truxenes 2ATPATrxSO$_2$ and 2DPATrxSO$_2$, followed by meta- and para-substituted truxene with carbazole 3CzTrxSO$_2$.

For the reduction potentials unsubstituted $TrxSO_2$ was also determined as a comparison. In general, three factors need to be considered: the strength of the donor (DPA or Cz), the position of the substituent (meta or para) and the influence of phenyl acetylene linker. Diphenylamine as the strongest donor shifts oxidation potential values to less positive while carbazole to more positive. Additionally, diphenyl amine linked by phenyl acetylene on the meta-position has only little (0.01 V) influence on the oxidation potential while the reduction potential is affected by 0.1 V. Interestingly, para-substituted truxene with carbazole shifts the first oxidation potential substantially from 0.88 V for $2CzTrxSO_2$ to 0.64 V for $3CzTrxSO_2$. Moreover, the second oxidation potential is observed for $3CzTrxSO_2$ at 0.92 V, which is close to the value of 0.88 V observed for $2CzTrxSO_2$ designating this oxidation to meta-substituted carbazole.

On the basis of the maximum of the potentials from SWV, the highest occupied molecular orbital (HOMO) and the lowest occupied molecular orbital (LUMO) energy levels were estimated and presented in **Table 4**.

2.6. Electroluminescence

The electroluminescence (EL) characteristics of using these materials as emitters were evaluated using multilayer OLEDs manufactured by spin-coating the hole injection and transport layers and evaporating the electron transport layer and cathode. The structure of the fabricated devices, shown in **Figure 4**, was as follows: ITO/PEDOT:PSS (40nm)/7 wt% CBP:$TrxSO_2$ (60 nm)/TPBI (60 nm)/LiF 0.7 (nm)/Al (100 nm). Where PEDOT:PSS (poly(3,4-ethylenedioxythiophene: poly(styerene sulfonate)) and CBP act as the hole injection layer and hole transporting layer, respectively, and TPBI 2,2',2''-(1,3,5-Benzinetriyl)-tris(1-phenyl-1-H-benzimidazole) as electron transporting layer. The electroluminescence (EL) spectra of the materials in devices are plotted in **Figure 5**a and they are almost identical to the PL data of the corresponding doped films. These emission peaks correspond to color

coordinates are presented in **Table 5** and **Figure 5**b. The truxene with two carbazole units has CIE coordinates at (0.16; 0.10) when adding additional carbazole units shifts CIEx coordinate to 0.17 while maintaing CIEy coordinate at the same value supporting above explanation of the weak interaction of *meta* substituted carbazole with truxene core. Presented results for $2CzTrxSO_2$ are close to NTSC and HDTV standards for blue emitters. Diphenyl- and triphenylamine based derivatives are much more shifted from these coordinates attaining sky-blue and green electroluminescence with CIE coordinates of (0.16, 0.34) and (0.22, 0.40), respectively. Graphs of external quantum efficiency (EQE) versus luminance and brightness versus voltage of the devices are displayed in Figure 3. Slightly higher voltages for deep blue OLEDs can be ascribed to the higher barrier for charge injection from the relatively low lying triplet level of CBP. Maximum efficiencies, at 100 and 1000 cd/m^2 recorded for the materials studied are 4.2, 3.7 and 2.6 % for $2CzTrxSO_2$; 3.9, 3.3 and 2.1 % $3CzTrxSO_2$; 10.6, 5.5 and 3.6 % for $2DPATrxSO_2$; 7.2, 7.0 and 6.0 % for $2ATPATrxSO_2$, respectively. Therefore, these materials give surprisingly low external quantum efficiency roll-off, as for donor-acceptor structures, down to 17% for ATPA and 38, 46 and 66 % two and three carbazole, and diphenylamine substituted truxene. These efficiencies are in agreement with the twice as high photoluminescence quantum yield of $2ATPATrxSO_2$, with a triphenylamine substituted core, while maintaining the similar fluorescence lifetime for all materials. Additionally, 2ATPATrxSO2 and $2DPATrxSO_2$ could still operate at brightness as high as 10 000 cd/m^2 with efficiencies of 3.4 and 2 %, respectively. The devices performance are presented in **Table 5**. The maximum theoretical EQE for OLEDs is expressed by below equation:

$$EQE = \beta \times \rho_{S/T} \times \rho_{PL} \times \eta_{out}$$

Where β is the charge balance factor (ideally equal to 1), $\rho_{S/T}$ is the fraction of radiative excitons (equal 0.25 for conventional fluorophores), ρ_{PL} is the fluorescence quantum yield and η_{out} is the light outcoupling efficiency (from 0.2 to 0.3). If the presented compounds were

standard fluorescent emitters, their EQE would be restricted to the 3.1%-4.6%, 1.8%-2.8%, 1.2%-1.8% and 1%-1.5% ranges for 2ATPATrxSO_2, 2DPATrxSO_2, 2CzTrxSO_2 and 3CzTrxSO_2, respectively. However, the observed EQE values of the devices were 2-3 times higher than those calculated based on 25% limitation of fluorescent emitters. Therefore, these results indicate that there is an enhancing mechanism involved in device operation. To test the presence of delayed components we measured time-resolved PL as discussed above. Since only ns excited state lifetime was observed this leaves two other possible explanations, as mentioned before HLCT and horizontal orientation of transition dipole moments. Where the former explanation is supported by short luminescence lifetime and the latter by presence of short contacts, showed in crystal structure, favouring horizontal orientation. To summarize, the above photophysical and electrical data show that these materials can be utilized as green, sky-blue and deep-blue emitters in OLEDs with potential HLCT excited state or, considering some previously reported truxene based materials properties,[82] also horizontal orientation of transition dipole moments can be expected.

2. Conclusion

In conclusion, four new green, sky-blue and deep-blue emitters for solution-processed OLEDs have been demonstrated. The efficiencies observed are two to three times higher than for conventional fluorescent emitters of the same photoluminescence quantum yield. Achieving EQE over 2% at luminance of 1000 cd/m^2 is extremely unusual for deep blue emitters based on donor-acceptor structure, especially with excellent thermal properties as compounds studied here. Additionally, two of studied materials can achieve high brightness, required for application in OLED lighting, with the efficiency up to 3.4 % at 10 000 cd/m^2. Therefore, our novel approach utilizing monothiatruxene shows a very promising strategy toward stable blue emitters with short luminescence lifetime.

3. Experimental Section

General: NMR spectra were recorded on a Bruker (400 and 500 MHz) spectrometers for solutions in $CDCl_3$. Chemical shifts are reported in parts per million. Chemical shifts multiplicities are reported as s: singlet, d: doublet, t: triplet, q: quartet, quint: quintet, and m: multiplet. Mass spectra (EI, ESI) were recorded with Xevo QTOF (Waters) high resolution, accurate mass tandem mass spectrometer equipped with Atmospheric Solids Analysis Probe (ASAP) and Bruker MicroToF 2. Elemental analysis was performed by Stephen Boyer of the Science Centre, London Metropolitan University using a Carlo Erba CE1108 Elemental Analyser.

Solution UV-visible absorption spectra were recorded using a Jasco V-670 UV/vis/NIR spectrophotometer controlled with SpectraManager software. Photoluminescence (PL) spectra were recorded with a Fluoromax-3 fluorimeter controlled by the ISAMain software. All samples were measured in a 1 cm cell at room temperature with dichloromethane as solvent. Quinine sulfate in 0.1 N H_2SO_4 (Φ= 0.51) was used as the standard for the fluorescence quantum yield determination, and a correction for solvent refractive index was made.

Films were prepared by spin-coating from dichloromethane solution at a concentration of 10 mg/ml onto quartz substrates with a spin speed of 2000 rpm. For blends the ratio of CBP to the studied material was 93:7 wt %. Photoluminescence spectra and quantum yields in thin film were recorded using an integrating sphere in a Hamamatsu C9920-02 measurement system.[83] Measurements were performed at room temperature and the integrating sphere was purged with nitrogen. The excitation wavelength was 325 nm or 380nm.

The fitting for the time-resolved photoluminescence is tri- (Fig. S2 and S3) and di-exponential (Fig. S4 and S5) fitting. The equation is expressed as y=y0+A1*exp(-x/t1)+A2*exp(-x/t2)+A3*exp(-x/t3). The average lifetime is calculated to be t=A1*t1+A2*t2+A3*t3, where A1+A2+A3=1.

All cyclic voltammetry measurements were carried out in freshly distilled CH_2Cl_2 using 0.3 M [TBA][PF_6] electrolyte in a three-electrode system, with each solution being purged with N_2 prior to measurement. The working electrode was a Pt disk. The reference electrode was Ag/AgCl and the counter electrode was a Pt rod. All measurements were made at room temperature using a mAUTOLAB Type III potentiostat, driven by the electrochemical software GPES. Cyclic voltammetry (CV) measurements used scan rates of 0.05 V s^{-1}; square wave voltammetry (SWV) was carried out at a step potential of 0.0021 V, square wave amplitude of 0.025 V, and a square wave frequency of 25 Hz giving a scan rate of 0.05 V s^{-1}. Ferrocene was used as the internal standard in each measurement.

Crystallographic data were collected using Agilent Technolo- gies SuperNovawithCuKa (l 141.54178 A) radiation at 120K. X-ray diffraction data were only observed up to a resolution of 1 Å and so the data set was cut at this resolution. This triggers a few checkCIF alerts. The model refines well, despite the weak data set.

Differential Differential scanning calorimetry (DSC) and Thermogravimetric analysis (TGA) were performed on NETZSCH STA 449F1 under nitrogen atmosphere in DSC/TG aluminium pan at a scan rate of 10 ºC/min.

Materials: All preparations were carried out using standard Schlenk line and air-sensitive chemistry techniques under nitrogen atmosphere. Tetrahydrofuran and dichloromethane were dried using a solvent purification system. Column chromatography was carried out using Silica 60A (particle size 35-70 μm, Fisher, UK) as the stationary phase, and TLC was performed on pre-coated silica gel plates (0.25 mm thick, 60 F254, Merck, Germany) and observed under UV light. Brominated monosulfonyltruxenes were synthesized according to procedure describe earlier.[59] All other materials were purchased from commercial suppliers and used without further purification.

*Synthetic procedure for dicarbazolo-monosulfonyltruxene (**2CzTrxSO$_2$**):* Dibrominated monosulfonyltruxene (0.120 g, 0.181 mmol), carbazole (0.076 g, 0.453 mmol), Pd2(dba)3 (0.007 g, 0.007 mmol), tri-o-tolylphosphine (0.111 g, 0.362 mmol) and NaOtBu (0.056 g, 0.579 mmol) were added to a oven dried Schlenk tube, backfilled with N_2 three times and left to dry under vacuum for 2 h. Dry toluene (8 mL) was added to the reaction mixture and the contents heated at 110°C in the dark for 48 h. The solvent was removed and the crude material was purified by column chromatography (SiO2, eluent: dichloromethane/petroleum ether 1/4 up to 1/2) to afford a slightly yellow solid 0.110g (73%). ^{1}H NMR (500 MHz, $CDCl_3$, δ ppm): 0.46 (t, *J*=7.5 Hz, 6H), 0.50 (t, *J*=7.3 Hz, 6H), 2.20–2.34 (m, 4H), 2.95–3.04 (m, 4H), 7.33–7.37 (m, 4H), 7.46–7.51 (m, 4H), 7.53 (d, *J*=8.2 Hz, 4H), 7.65 (t, *J*=7.4 Hz, 1H), 7.69 (d, J=1.8 Hz, 1H), 7.80–7.71 (m, 4H), 8.06 (dd, *J*=7.6, 1.2 Hz, 1H), 8.20 (dd, *J*=7.7, 4.4 Hz, 4H), 8.49 (d, *J*=8.2 Hz, 1H), 8.58 (d, *J*=9.0 Hz, 1H), 9.01 (d, *J*=8.3 Hz, 1H). ^{13}C NMR (126 MHz, $CDCl_3$, δ ppm): 9.11 (CH_3), 9.22 (CH_3), 29.73 (CH_2), 29.94 (CH_2), 57.85 (C-$(CH_2)_2$), 58.90 (C-$(CH_2)_2$), 109.85 (C_{Ar}-H), 110.01 (C_{Ar}-H), 120.32 (C_{Ar}-H), 120.51 (C_{Ar}-H), 120.58 (C_{Ar}-H), 120.69 (C_{Ar}-H), 120.75 (C_{Ar}-H), 121.16 (C_{Ar}-H), 122.87 (C_{Ar}-H), 123.75 (C_{Ar}), 123.83 (C_{Ar}), 125.83 (C_{Ar}-H), 126.30 (C_{Ar}-H), 126.34 (C_{Ar}-H), 126.70 (C_{Ar}-H), 126.74 (C_{Ar}-H), 127.64 (C_{Ar}-H), 128.39 (C_{Ar}), 129.91 (C_{Ar}-H), 130.15 (C_{Ar}), 131.83 (C_{Ar}), 133.69 (C_{Ar}-H), 135.73 (C_{Ar}), 137.31 (C_{Ar}), 138.16 (C_{Ar}), 138.42 (C_{Ar}),138.88 (C_{Ar}), 139.41 (C_{Ar}), 140.88 (C_{Ar}), 140.99 (C_{Ar}), 144.89 (C_{Ar}), 145.86 (C_{Ar}), 146.68 (C_{Ar}), 154.45 (C_{Ar}), 155.50 (C_{Ar}). MS (ESI): m/z (%)= 852.27 [$(M+H_2O)^+$, 100]; 857.32 [$(M+Na)^+$, 70]; 835.34 [$(M+H)^+$, 65]. Anal. calcd for $C_{58}H_{46}N_2O_2S$: C 83.42, H 5.55, N 3.35; found: C 83.15, H 5.51, N 3.35.

*Synthetic procedure for bidiphenylamine-monosulfonyltruxene (**2DPATrxSO$_2$**):* Dibrominated monosulfonyltruxene (0.120 g, 0.181 mmol), diphenylamine (0.058 g, 0.340 mmol), $Pd_2(dba)_3$ (0.005 g, 0.006 mmol), tri-o-tolylphosphine (0.083 g, 0.272 mmol) and NaO^{t}Bu

(0.042 g, 0.435 mmol) were added to a dried Schlenk tube, backfilled with N_2 three times and left to dry under vacuum for 2 h. Dry toluene (5 mL) was added to the reaction mixture and the contents heated at 110 °C in the dark for 48 h. The solvent was removed and the crude material was purified by column chromatography (SiO_2, eluent: dichloromethane/petroleum ether 1/4 up to 1/1) to afford a yellow solid 0.110g (72%). ^{1}H NMR (500 MHz, $CDCl_3$, δ ppm): 0.33 (t, *J*=7.3 Hz, 12H), 1.90–2.03 (m, 4H), 2.64–2.83 (m, 4H), 7.03–7.21 (m, 16H), 7.27–7.34 (m, 8H), 7.54 (t, *J*=7.5 Hz, 1H), 7.66 (dd, *J*=11.3, 4.3 Hz, 1H), 7.96 (dd, *J*=7.6, 1.2 Hz, 1H), 8.08 (d, *J*=8.7 Hz, 1H), 8.36 (d, *J*=8.2 Hz, 1H), 8.55 (d, *J*=8.5 Hz, 1H). ^{13}C NMR (126 MHz, $CDCl_3$, δ ppm): 9.01 (CH_3), 9.07 (CH_3), 29.49 (CH_2), 29.59 (CH_2), 57.18 (C-$(CH_2)_2$), 58.18 (C-$(CH_2)_2$), 116.35 (C_{Ar}-H), 116.71 (C_{Ar}-H), 121.66 (C_{Ar}-H), 122.56 (C_{Ar}-H), 123.15 (C_{Ar}-H), 123.30 (C_{Ar}-H), 123.66 (C_{Ar}-H), 124.77 (C_{Ar}-H), 125.03 (C_{Ar}-H), 125.45 (C_{Ar}), 125.92 (C_{Ar}-H), 126.23 (C_{Ar}-H), 127.50 (C_{Ar}-H), 127.52 (C_{Ar}), 127.62 (C_{Ar}), 128.38 (C_{Ar}-H), 129.19 (C_{Ar}-H), 129.32 (C_{Ar}-H), 129.46 (C_{Ar}-H), 129.58 (C_{Ar}-H), 131.20 (C_{Ar}), 132.26 (C_{Ar}), 132.49 (C_{Ar}), 133.22 (C_{Ar}-H), 138.38 (C_{Ar}), 139.87 (C_{Ar}), 144.16 (C_{Ar}), 145.04 (C_{Ar}), 145.16 (C_{Ar}), 147.59 (C_{Ar}), 147.79 (C_{Ar}), 148.56 (C_{Ar}), 149.16 (C_{Ar}), 154.02 (C_{Ar}), 154.86 (C_{Ar}). MS (ESI): m/z (%)= 838.36 [$(M)^+$, 100]. Anal. calcd for $C_{74}H_{58}N_2O_2S$: C 85.52, H 5.62, N 2.70; found: C 85.23, H 5.89, N 2.77.

*Synthetic procedure for di(4-ethynylphenyl)-diphenylamine-monosulfonyltruxene (**2ATPATrxSO$_2$**):* Dibrominated monosulfonyltruxene (0.080 g, 0.121 mmol), (4-ethynyl-phenyl)-diphenyl-amine (0.091 g, 0.338 mmol), $Pd(PPh_3)_2Cl_2$ (0.005 g, 0.007 mmol), PPh_3 (0.004 g, 0.015 mmol) and CuI (0.006 g, 0.029 mmol) were added to a dried Schlenk tube, backfilled with N_2 three times and left to dry under vacuum for 2 h. Piperidine (0.1 mL, 0.968 mmol) and dry toluene (4 mL) were added to the reaction mixture and it was heated at 90 °C for 19 h. The solvent was removed and the crude material was purified by column chromatography (SiO_2, eluent: dichloromethane/petroleum ether 1/4 up to 1/2) to afford a yellow-orange solid 0.087g (86%). ^{1}H NMR (500 MHz, $CDCl_3$, δ ppm): 0.31 (t, *J*=7.33 Hz,

12H), 2.16–2.30 (m, 4H), 2.83–2.94 (m, 4H), 7.02–7.11 (m, 8H), 7.12–7.17 (m, 8H), 7.27–7.33 (m, 8H), 7.42–7.46 (m, 4H), 7.56–7.66 (m, 5H), 7.73 (t, *J*=7.5 Hz, 1H), 8.00 (dd, *J*=7.6, 1.2 Hz, 1H), 8.31 (d, *J*=8.3 Hz, 1H), 8.45 (d, *J*=8.2 Hz, 1H), 8.70 (d, *J*=8.2 Hz, 1H). ^{13}C NMR (126 MHz, $CDCl_3$, δ ppm): 8.91 (CH_3), 8.99 (CH_3), 29.70 (CH_2), 29.88 (CH_2), 57.56 ($\underline{C}$-$(CH_2)_2$), 58.54 ($\underline{C}$-$(CH_2)_2$), 88.91 (C≡C), 88.49(C≡C), 91.23(C≡C), 91.71(C≡C), 115.74 (C_{Ar}), 116.08 (C_{Ar}), 122.26 (C_{Ar}-H), 122.39 (C_{Ar}-H), 122.71 (C_{Ar}-H), 123.75 (C_{Ar}-H), 123.87 (C_{Ar}-H), 124.10 (C_{Ar}), 124.55 (C_{Ar}), 125.08 (C_{Ar}-H), 125.10 (C_{Ar}-H), 125.21 (C_{Ar}-H), 125.28 (C_{Ar}-H), 125.48 (C_{Ar}-H), 127.55 (C_{Ar}-H), 128.18 (C_{Ar}), 128.38 (C_{Ar}), 129.57 (C_{Ar}-H), 129.60 (C_{Ar}-H), 129.73 (C_{Ar}-H), 129.94 (C_{Ar}), 130.51 (C_{Ar}-H), 131.25 (C_{Ar}-H), 131.85 (C_{Ar}), 132.79 (C_{Ar}-H), 133.52 (C_{Ar}-H), 136.40 (C_{Ar}), 138.07 (C_{Ar}), 138.15 (C_{Ar}), 139.49 (C_{Ar}), 145.04 (C_{Ar}), 145.78 (C_{Ar}), 146.68 (C_{Ar}), 147.28 (C_{Ar}), 147.35 (C_{Ar}), 148.21 (C_{Ar}), 148.38 (C_{Ar}), 152.50 (C_{Ar}), 153.44 (C_{Ar}). MS (ESI): m/z (%)= 1061.41 [$(M+Na)^+$, 55], 1039.43 [$(M+H)^+$, 50]. Anal. calcd for $C_{74}H_{58}N_2O_2S$: C 85.52, H 5.62, N 2.70; found, C 85.23, H 5.89, N 2.77.

*Synthetic procedure for tricarbazolo-monosulfonyltruxene (**3CzTrxSO$_2$**):* Tribrominated monosulfonyltruxene (0.045 g, 0.061 mmol), carbazole (0.033 g, 0.200 mmol), $Pd_2(dba)_3$ (0.002 g, 0.003 mmol), tri-o-tolylphosphine (0.056 g, 0.182 mmol) and NaO^tBu (0.028 g, 0.291 mmol) were added to a dried Schlenk tube, backfilled with N_2 three times and left to dry under vacuum for 2 h. Dry toluene (3 mL) was added to the reaction mixture and the contents heated at 110 °C in the dark for 44 h. The solvent was removed and the crude material was purified by column chromatography (SiO_2, eluent: dichloromethane/petroleum ether 1/5 up to 1/2) to afford a slightly yellow solid 0.032g (53%). ^{1}H NMR (500 MHz, $CDCl_3$, δ ppm): 0.48 (t, *J*=7.3 Hz, 6H), 0.52 (t, *J*=7.3 Hz, 6H), 2.07–2.16 (m, 2H), 2.27–2.38 (m, 2H), 2.72–2.83 (m, 2H), 2.97–3.08 (m, 2H), 7.30–7.58 (m, 18H), 7.63 (d, *J*=2.0 Hz, 1H), 7.70–7.75 (m, 2H), 7.80 (dd, *J*=8.3, 1.9 Hz, 1H), 7.89 (dd, *J*=8.0, 1.3 Hz, 1H), 8.17 (d, *J*=7.8

Hz, 2H), 8.21 (d, *J*=7.8 Hz, 4H), 8.30 (d, *J*=8.0 Hz, 1H), 8.58 (d, *J*=8.6 Hz, 1H), 8.67 (d, *J*=1.0 Hz, 1H), 9.05 (d, *J*=8.3 Hz, 1H).

^{13}C NMR (126 MHz, $CDCl_3$, δ ppm): 9.12 (CH_3), 9.23 (CH_3), 29.92 (CH_2), 30.05 (CH_2), 57.81 ($\underline{C}$-$(CH_2)_2$), 59.01 ($\underline{C}$-$(CH_2)_2$), 109.59 (C_{Ar}-H), 109.79 (C_{Ar}-H), 110.00 (C_{Ar}-H), 120.38 (C_{Ar}-H), 120.55 (C_{Ar}-H), 120.62 (C_{Ar}-H), 120.66 (C_{Ar}-H), 120.82 (C_{Ar}-H), 120.93 (C_{Ar}-H), 121.03 (C_{Ar}-H), 121.27 (C_{Ar}-H) 123.79 (C_{Ar}), 123.84 (C_{Ar}), 124.27 (C_{Ar}), 124.40 (C_{Ar}-H), 125.80 (C_{Ar}-H), 126.05 (C_{Ar}-H), 126.33 (C_{Ar}-H), 126.64 (C_{Ar}-H), 126.78 (C_{Ar}-H), 127.56 (C_{Ar}), 127.93 (C_{Ar}-H), 130.47 (C_{Ar}), 134.18 (C_{Ar}), 135.52 (C_{Ar}), 136.14 (C_{Ar}), 136.94 (C_{Ar}), 138.61 (C_{Ar}), 139.10 (C_{Ar}), 139.64 (C_{Ar}), 140.30 (C_{Ar}), 140.71 (C_{Ar}), 140.97 (C_{Ar}), 142.91 (C_{Ar}), 145.09 (C_{Ar}), 146.24 (C_{Ar}), 147.28 (C_{Ar}), 154.53 (C_{Ar}), 155.38 (C_{Ar}). MS (ESI): m/z (%)=1022.38 [(M+Na)+, 100]; 1000.39 [(M+H)+, 25]. Anal. calcd for $C_{70}H_{53}N_3O_2S$: C 84.05, H 5.34, N 4.20; found: C 83.89, H 5.47, N 4.29.

OLED fabrication and measurements: OLEDs were fabricated on 12 mm x 12 mm indium tin oxide (ITO) coated glass substrates. The ITO had a thickness of 140 nm and a sheet resistance of less than 15 Ω/sq. The ITO had been etched with 37% HCl and zinc powder to provide an active area of 6 mm^2 and then cleaned by ultrasound in acetone and 2-propanol for 15 minutes each. Before spin-coating, the substrates were ashed by an oxygen plasma for 5 minutes. A layer of Poly(3,4-ethylenedioxythiophene):poly(styrenesulfonate) (PEDOT:PSS) with a thickness of 40 nm was first spin-coated on the ITO and baked on a hotplate at 120°C for 10 minutes. A layer of CBP:TrxSO_2 layer with a thickness of 60 nm was spin-coated from dichloromethane at a concentration of 10 mg/ml on the PEDOT layer. The samples were then transferred to a vacuum evaporation system. A layer of 1,3,5-tris(2-N-phenylbenzimidazolyl)benzene (TPBI) with a thickness of 60 nm was deposited through a shadow mask at a pressure of ~10^{-6} mbar and then a layer of LiF with a thickness of 0.7 nm and a layer of aluminum with a thickness of more than 100 nm were subsequently deposited

as the cathode. The samples were then encapsulated with optical curing adhesive and coverslips in a nitrogen glove box. The OLEDs were measured in a vacuum chamber. The efficiency was obtained by measuring the light output in the forward direction with a photodiode and assuming Lambertian emission. An Andor DV420-BV CCD spectrometer was used to measure the electroluminescence (EL) spectra. Current-voltage-brightness data were collected using Keithley 2400 source-meter and Keithley 2000 multi-meter units. A Veeco DekTak 150 surface profilometer was used for measuring the layer thicknesses.

[CCDC 1875407 contains the supplementary crystallographic data for this paper. These data can be obtained free of charge from The Cambridge Crystallographic Data Centre via www.ccdc.cam.ac.uk/data_request/cif.]

Supporting Information
Supporting Information is available from the Wiley Online Library or from the author.

Acknowledgements

M.R.M. and S.Z. contributed equally to this work. We thank the Mazowieckie voivodeship, co-financed with the European Union funds by the European Social Fund and European Union's Horizon 2020 Research and Innovation Programme H2020-MSCA-IF-2014-659237 for financial support. We thank Dr. Gary Nichol for the crystallographic data collection and refinement; The University of Edinburgh for funding the diffractometer purchase. I.D.W.S. acknowledges support from a Royal Society Wolfson Research Merit Award and from the Engineering and Physical Sciences Research Council (grant EP/J009016/1).

Received: ((will be filled in by the editorial staff))
Revised: ((will be filled in by the editorial staff))
Published online: ((will be filled in by the editorial staff))

References

[1] X. Zhang, J. Yin, J. Yoon, *Chem. Rev.* **2014**, *114*, 4918.

[2] K. P. Carter, A. M. Young, A. E. Palmer, *Chem. Rev.* **2014**, *114*, 4564.

[3] K. K.-W. Lo, S. P.-Y. Li, *RSC Adv.* **2014**, *4*, 10560.

[4] E. Pazos, M. E. Vázquez, *Biotechnol. J.* **2014**, *9*, 241.

[5] V. N. Mehta, S. K. Kailasa, H.-F. Wu, *J. Nanosci. Nanotechnol.* **2014**, *14*, 447.

[6] N. Hildebrandt, K. D. Wegner, W. R. Algar, *Coord. Chem. Rev.* **2014**, *273–274*, 125.

[7] N. Frascione, J. Gooch, B. Daniel, *Analyst* **2013**, *138*, 7279.

[8] E. Hemmer, N. Venkatachalam, H. Hyodo, A. Hattori, Y. Ebina, H. Kishimoto, K. Soga, *Nanoscale* **2013**, *5*, 11339.

[9] O. Akinfieva, I. Nabiev, A. Sukhanova, *Crit. Rev. Oncol. Hematol.* **2013**, *86*, 1.

[10] C. W. Lee, O. Y. Kim, J. Y. Lee, *J. Ind. Eng. Chem.* **2014**, *20*, 1198.

[11] N. Thejokalyani, S. J. Dhoble, *Renew. Sustain. Energy Rev.* **2014**, *32*, 448.

[12] C. Adachi, *Jpn. J. Appl. Phys.* **2014**, *53*, 060101.

[13] H. Sasabe, J. Kido, *European J. Org. Chem.* **2013**, *2013*, 7653.

[14] J. Wang, F. Zhang, J. Zhang, W. Tang, A. Tang, H. Peng, Z. Xu, F. Teng, Y. Wang, *J. Photochem. Photobiol. C Photochem. Rev.* **2013**, *17*, 69.

[15] X. Guo, M. Baumgarten, K. Müllen, *Prog. Polym. Sci.* **2013**, *38*, 1832.

[16] J. Roncali, P. Leriche, P. Blanchard, *Adv. Mater.* **2014**, *26*, 3821.

[17] N. Agnihotri, *J. Photochem. Photobiol. C Photochem. Rev.* **2014**, *18*, 18.

[18] Y. Fu, F. Wang, Y. Zhang, X. Fang, W. Lai, W. Huang, *Acta Chim. Sin.* **2014**, *72*, 158.

[19] K. Nakabayashi, H. Mori, *Materials (Basel).* **2014**, *7*, 3274.

[20] L. Dou, J. You, Z. Hong, Z. Xu, G. Li, R. A. Street, Y. Yang, *Adv. Mater.* **2013**, *25*, 6642.

[21] M. A. Baldo, D. F. O'Brien, M. E. Thompson, S. R. Forrest, *Phys. Rev. B* **1999**, *60*, 14422.

[22] M. A. Baldo, D. F. O'Brien, Y. You, A. Shoustikov, S. Sibley, M. E. Thompson, S. R. Forrest, **1998**, *395*, 151.

[23] C. Adachi, M. a. Baldo, M. E. Thompson, S. R. Forrest, *J. Appl. Phys.* **2001**, *90*, 5048.

[24] L. Xiao, S.-J. Su, Y. Agata, H. Lan, J. Kido, *Adv. Mater.* **2009**, *21*, 1271.

[25] D. Y. Kondakov, T. D. Pawlik, T. K. Hatwar, J. P. Spindler, *J. Appl. Phys.* **2009**, *106*, 124510.

[26] J. Zhou, P. Chen, X. Wang, Y. Wang, Y. Wang, F. Li, M. Yang, Y. Huang, J. Yu, Z. Lu, *Chem. Commun. (Camb).* **2014**, *50*, 7586.

[27] C.-J. Chiang, A. Kimyonok, M. K. Etherington, G. C. Griffiths, V. Jankus, F. Turksoy, A. P. Monkman, *Adv. Funct. Mater.* **2013**, *23*, 739.

[28] P.-Y. Chou, H.-H. Chou, Y.-H. Chen, T.-H. Su, C.-Y. Liao, H.-W. Lin, W.-C. Lin, H.-Y. Yen, I.-C. Chen, C.-H. Cheng, *Chem. Commun. (Camb).* **2014**, *50*, 6869.

[29] H. Uoyama, K. Goushi, K. Shizu, H. Nomura, C. Adachi, *Nature* **2012**, *492*, 234.

[30] A. Endo, K. Sato, K. Yoshimura, T. Kai, A. Kawada, H. Miyazaki, C. Adachi, *Appl. Phys. Lett.* **2011**, *98*, 083302.

[31] T. Nishimoto, T. Yasuda, S. Y. Lee, R. Kondo, C. Adachi, *Mater. Horiz.* **2014**, *1*, 264.

[32] H. Wang, L. Xie, Q. Peng, L. Meng, Y. Wang, Y. Yi, P. Wang, *Adv. Mater.* **2014**, *26*, 5198.

[33] S. Youn Lee, T. Yasuda, H. Nomura, C. Adachi, *Appl. Phys. Lett.* **2012**, *101*, 093306.

[34] T. Nakagawa, S.-Y. Ku, K.-T. Wong, C. Adachi, *Chem. Commun. (Camb).* **2012**, *48*, 9580.

[35] Q. Zhang, J. Li, K. Shizu, S. Huang, S. Hirata, H. Miyazaki, C. Adachi, *J. Am. Chem. Soc.* **2012**, *134*, 14706.

[36] G. Méhes, H. Nomura, Q. Zhang, T. Nakagawa, C. Adachi, *Angew. Chem. Int. Ed. Engl.* **2012**, *51*, 11311.

[37] H. Tanaka, K. Shizu, H. Miyazaki, C. Adachi, *Chem. Commun. (Camb).* **2012**, *48*, 11392.

[38] J. Li, T. Nakagawa, J. MacDonald, Q. Zhang, H. Nomura, H. Miyazaki, C. Adachi, *Adv. Mater.* **2013**, *25*, 3319.

[39] K. Sato, K. Shizu, K. Yoshimura, A. Kawada, H. Miyazaki, C. Adachi, *Phys. Rev. Lett.*

2013, *110*, 247401.

[40] J. Lee, K. Shizu, H. Tanaka, H. Nomura, T. Yasuda, C. Adachi, *J. Mater. Chem. C* **2013**, *1*, 4599.

[41] W. Li, Y. Pan, R. Xiao, Q. Peng, S. Zhang, D. Ma, F. Li, F. Shen, Y. Wang, B. Yang, Y. Ma, *Adv. Funct. Mater.* **2014**, *24*, 1609.

[42] T. D. Schmidt, T. Lampe, M. R. Daniel Sylvinson, P. I. Djurovich, M. E. Thompson, W. Brütting, *Phys. Rev. Appl.* **2017**, *8*.

[43] J. Frischeisen, D. Yokoyama, A. Endo, C. Adachi, W. Brütting, *Org. Electron. physics, Mater. Appl.* **2011**, *12*, 809.

[44] D. Yokoyama, *J. Mater. Chem.* **2011**, *21*, 19187.

[45] L. Zhao, T. Komino, M. Inoue, J.-H. Kim, J. C. Ribierre, C. Adachi, *Appl. Phys. Lett.* **2015**, *106*, 063301.

[46] A. Graf, P. Liehm, C. Murawski, S. Hofmann, K. Leo, M. C. Gather, *J. Mater. Chem. C* **2014**, *2*, 10298.

[47] S. Reineke, K. Walzer, K. Leo, *Phys. Rev. B* **2007**, *75*, 125328.

[48] M. A. Baldo, C. Adachi, S. R. Forrest, *Phys. Rev. B* **2000**, *62*, 10967.

[49] J. Lee, C. H. Park, J. Kwon, S. C. Yoon, L.-M. Do, C. Lee, *Synth. Met.* **2012**, *162*, 1961.

[50] K. Saxena, V. K. Jain, D. S. Mehta, *Opt. Mater. (Amst).* **2009**, *32*, 221.

[51] M. C. Gather, S. Reineke, *J. Photonics Energy* **2015**, *5*, 57607.

[52] K.-H. Kim, S. Lee, C.-K. Moon, S.-Y. Kim, Y.-S. Park, J.-H. Lee, J. Woo Lee, J. Huh, Y. You, J.-J. Kim, *Nat. Commun.* **2014**, *5*, 4769.

[53] T.-A. Lin, T. Chatterjee, W.-L. Tsai, W.-K. Lee, M.-J. Wu, M. Jiao, K.-C. Pan, C.-L. Yi, C.-L. Chung, K.-T. Wong, C.-C. Wu, *Adv. Mater.* **2016**, *28*, 6976.

[54] W. Zeng, H.-Y. Lai, W.-K. Lee, M. Jiao, Y.-J. Shiu, C. Zhong, S. Gong, T. Zhou, G. Xie, M. Sarma, K.-T. Wong, C.-C. Wu, C. Yang, *Adv. Mater.* **2018**, *30*, 1704961.

[55] H. K. Bisoyi, S. Kumar, *Chem. Soc. Rev.* **2010**, *39*, 264.

[56] H. L. Ni, H. Monobe, P. Hu, B. Q. Wang, Y. Shimizu, K. Q. Zhao, *Liq. Cryst.* **2013**, *40*, 411.

[57] K. Zhao, C. Chen, H. Monobe, P. Hu, B. Wang, Y. Shimizu, **2011**, 1.

[58] F. Goubard, F. Dumur, *RSC Adv.* **2015**, *5*, 3521.

[59] M. R. Maciejczyk, J. A. G. Williams, N. Robertson, M. Pietraszkiewicz, *RSC Adv.* **2017**, *7*, 49532.

[60] P. L. dos Santos, J. S. Ward, D. G. Congrave, A. S. Batsanov, J. Eng, J. E. Stacey, T. J. Penfold, A. P. Monkman, M. R. Bryce, *Adv. Sci.* **2018**, *5*, 1700989.

[61] Y. Xie, X. Zhang, Y. Xiao, Y. Zhang, F. Zhou, J. Qi, J. Qu, *Chem. Commun. (Camb).* **2012**, *48*, 4338.

[62] X.-Y. Cao, X.-H. Liu, X.-H. Zhou, Y. Zhang, Y. Jiang, Y. Cao, Y.-X. Cui, J. Pei, *J. Org. Chem.* **2004**, *69*, 6050.

[63] Z. Yang, B. Xu, J. He, L. Xue, Q. Guo, H. Xia, W. Tian, *Org. Electron.* **2009**, *10*, 954.

[64] M. Kimura, S. Kuwano, Y. Sawaki, H. Fujikawa, K. Noda, Y. Taga, K. Takagi, *J. Mater. Chem.* **2005**, *15*, 2393.

[65] Y. M. Sun, K. Xiao, Y. Q. Liu, J. L. Wang, J. Pei, G. Yu, D. B. Zhu, *Adv. Funct. Mater.* **2005**, *15*, 818.

[66] X. Zong, M. Liang, C. Fan, K. Tang, G. Li, Z. Sun, S. Xue, *J. Phys. Chem. C* **2012**, *116*, 11241.

[67] G. Tsiminis, Y. Wang, P. E. Shaw, A. L. Kanibolotsky, I. F. Perepichka, M. D. Dawson, P. J. Skabara, G. a. Turnbull, I. D. W. Samuel, *Appl. Phys. Lett.* **2009**, *94*, 243304.

[68] H.-J. Xu, B. Du, C. P. Gros, P. Richard, J.-M. Barbe, P. D. Harvey, *J. Porphyr. Phthalocyanines* **2013**, *17*, 44.

[69] M.-S. Yuan, Z.-Q. Liu, Q. Fang, *J. Org. Chem.* **2007**, *72*, 7915.

[70] K. Górski, J. Mech-Piskorz, K. Noworyta, B. Leśniewska, M. Pietraszkiewicz, *New J. Chem.* **2018**, *42*, 5844.

[71] Y. Li, J. Y. Liu, Y. Di Zhao, Y. C. Cao, *Mater. Today* **2017**, *20*, 258–266.

[72] M. Y. Wong, E. Zysman-Colman, *Adv. Mater.* **2017**, *29*, 1605444.

[73] Q. Zhang, J. Li, K. Shizu, S. Huang, S. Hirata, H. Miyazaki, C. Adachi, *J. Am. Chem. Soc.* **2012**, *134*, 14706.

[74] T.-T. Bui, F. Goubard, M. Ibrahim-Ouali, D. Gigmes, F. Dumur, T.-T. Bui, F. Goubard, M. Ibrahim-Ouali, D. Gigmes, F. Dumur, *Appl. Sci.* **2018**, *8*, 494.

[75] E. Lee, S. Lee, S. Y. Kim, J.-H. Chong, B. H. Choi, J. H. Lee, S. Kim, *J. Inf. Disp.* **2016**, *17*, 151.

[76] K.-H. Lin, A. Prlj, C. Corminboeuf, *J. Phys. Chem. C* **2017**, *121*, 21729.

[77] M. Pietraszkiewicz, M. Maciejczyk, I. D. W. Samuel, S. Zhang, *J. Mater. Chem. C* **2013**, *1*, 8028.

[78] S. Yin, A. Z. Shuai,, Y. Wang, **2003**, *43*, 970.

[79] S. Jang, S. H. Han, J. Y. Lee, Y. Lee, *Synth. Met.* **2018**, *239*, 43.

[80] K.-H. Lin, A. Prlj, C. Corminboeuf, *J. Phys. Chem. C* **2017**, *121*, 21729.

[81] T. Chen, L. Zheng, J. Yuan, Z. An, R. Chen, Y. Tao, H. Li, X. Xie, W. Huang, *Sci. Rep.* **2015**, *5*.

[82] K. Rakstys, S. Paek, P. Gao, P. Gratia, T. Marszalek, G. Grancini, K. T. Cho, K. Genevicius, V. Jankauskas, W. Pisula, M. K. Nazeeruddin, *J. Mater. Chem. A* **2017**, *5*, 7811.

[83] N. C. Greenham, I. D. W. Samuel, G. R. Hayes, R. T. Phillips, Y. A. R. R. Kessener, S. C. Moratti, A. B. Holmes, R. H. Friend, *Chem. Phys. Lett.* **1995**, *241*, 89.

Table 1. OLED characteristics of deep blue emitters.

Entry	Structure	$EQE_{max/100/1000}$ [%]	RO_{1000} [%][a)]	CIE (x, y)	Reference
1	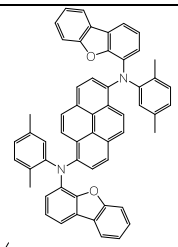	$7.7/-/7.3_{EQE500}$	5_{500}	(0.14, 0.10)	[84]
2	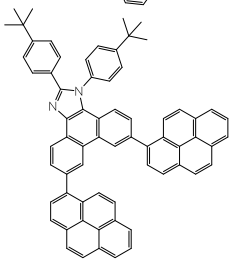	5.8/5.7/5.8	0	(0.15, 0.10)	[85]
3	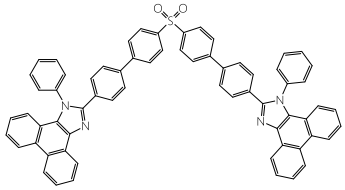	6.8/-/5.6	18	(0.15, 0.08)	[86]
4	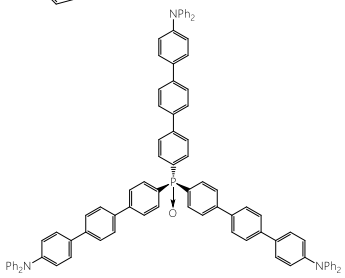	6.5/6.0/-	8_{100}	(0.15, 0.06)	[87]
5	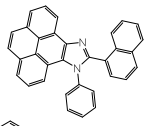	5.05/5.05/4.67	8	(0.16, 0.06)	[88]
6	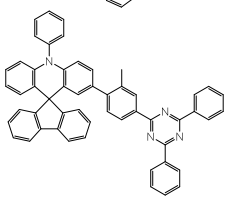	6.2/3.4/-	45_{500}	(0.15, 0.10)	[89]

7	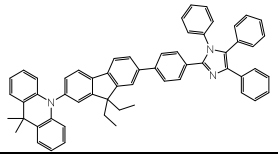	4.56/-/1.8	61	(0.15, 0.06)	[90]

[a]EQE roll-off from maximum value to that at 1000 cd/m^2 or at the brightness stated at the subscript, determined by (EQE_{max}-EQE_{1000})/EQE_{max}.

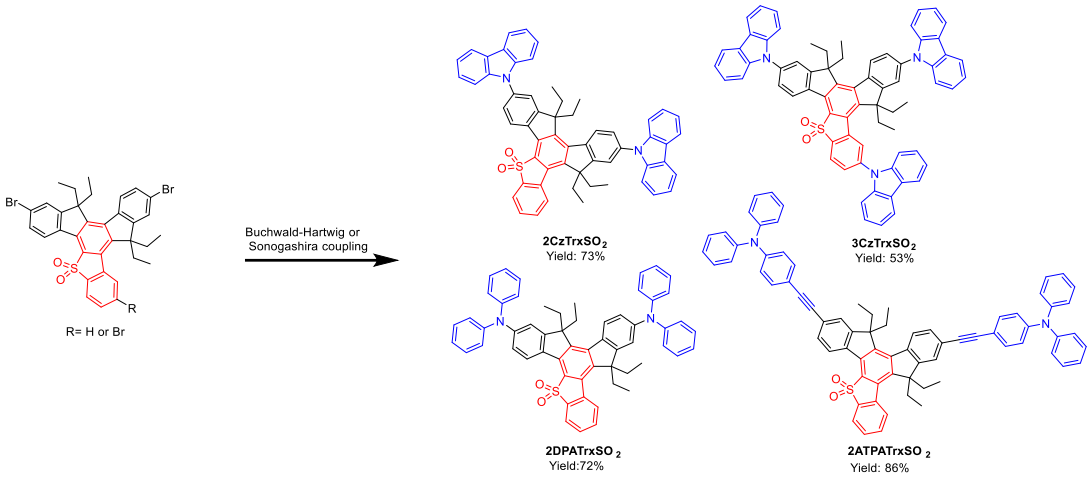

Scheme 1. Synthesis of Monothiatruxene based emitters: 2DPATrxSO$_2$, 2ATPATrxSO$_2$, 2CzTrxSO$_2$ and 2CzTrxSO$_2$.

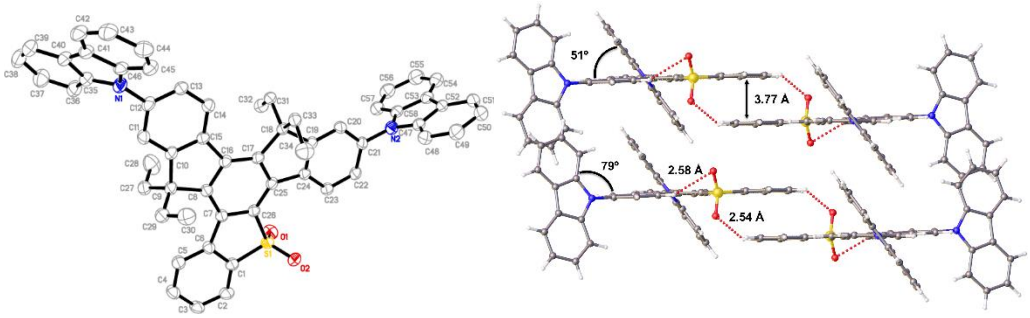

Figure 1. The molecular structure (left) and crystal packing (right) of 2CzTrxSO$_2$.

Table 2. Thermal properties.

Compound	Molecular weight [g/mol]	Glass transition temperature[a] [ºC]	Melting point[b] [ºC]	Decomposition temperature[b] [ºC]	Residual mass at 500 ºC[b] [%]
2DPATrxSO$_2$	838.36	171	-	352	64
2ATPATrxSO$_2$	1039.35	336	-	442	86
2CzTrxSO$_2$	835.08	259	-	431	82
3CzTrxSO$_2$	1000.27	248	398	427	82

[a]Determined by DSC; [b]Determined by TGA.

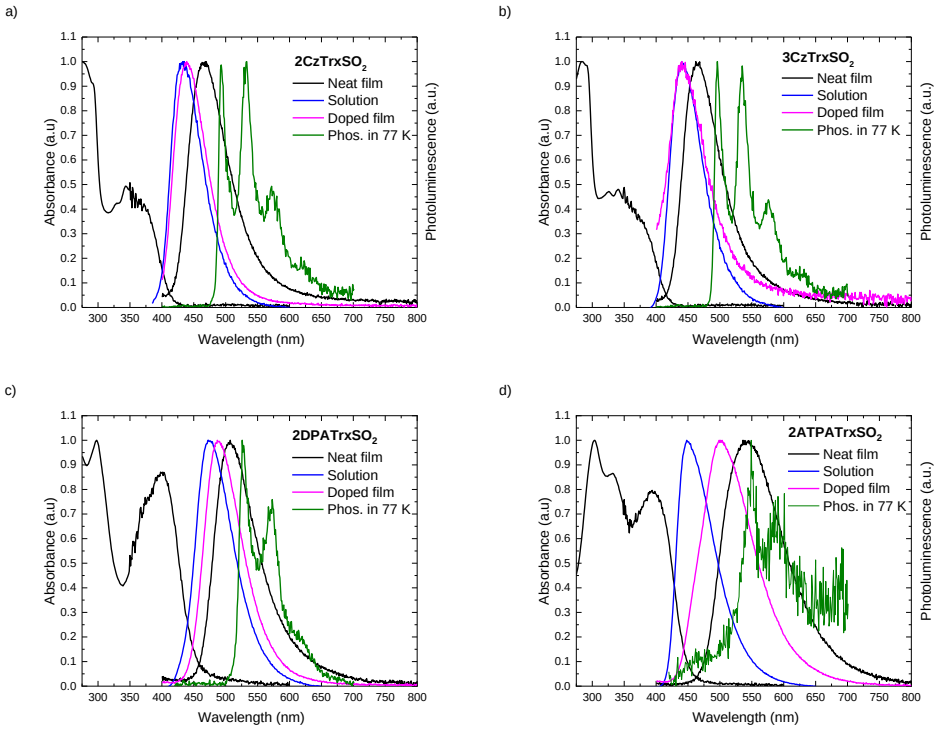

Figure 2. UV-VIS absorption and photoluminescence spectra of studied emitters in neat films, doped films and toluene solutions at r.t. and 77 K.

Table 3. Photophysical properties.

Emitter		λ_{abs} [d] [nm]	λ_{PL} [e] [nm]	Φ_{air} [f] [%]	$\Phi_{deaerated}$ [f] [%]	$\tau_{vac.}$ [g] [ns]	τ_{air} [g] [ns]	E_{S1} [h] [eV]	E_{T1} [h] [eV]	ΔE_{ST} [i] [eV]
$2DPATrxSO_2$	Sol[a]	-	475	19	20	1.68	-	2.61	2.37	0.24
	Dope[b]	-	475	-	37	-	-	-	-	-
	Neat[c]	400	510	-	19	2.21	1.99	-	-	-
$2ATPATrxSO_2$	Sol[a]	-	450	58	62	1.55	-	2.76	2.30	0.46
	Dope[b]	-	500	-	62	-	-	-	-	-
	Neat[c]	394	540	-	25	2.63	2.61	-	-	-
$2CzTrxSO_2$	Sol[a]	-	430	25	25	1.83	-	2.88	2.54	0.34
	Dope[b]	-	440	-	24	-	-	-	-	-
	Neat[c]	350	460	-	17	11.42	3.59	-	-	-
$3CzTrxSO_2$	Sol[a]	-	440	21	21	1.66	-	2.82	2.52	0.30
	Dope[b]	-	440	-	20	-	-	-	-	-

Neat[c)]	350	460	-	14	6.56	5.81	-	-	-

[a)]Measured in oxygen-free toluene solution; [b)]Measured as a doped CBP film (with 7 wt %); [c)]Measured as a pristine neat film [d)]Absorption maximum wavelength; [e)]Fluorescence maximum wavelength; [f)]Photoluminescence quantum yield evaluated usinga and integrating sphere under N_2; [g)]Photoluminescence lifetime measured in neat powders, an average lifetime has been quoted; [h)]Singlet and triplet excited energies estimated from the onset and maximum peak wavelengths of emission spectra in toluene solution at 300 and 77 K, respectively;
i) $\Delta E_{ST} = E_S - E_T$.

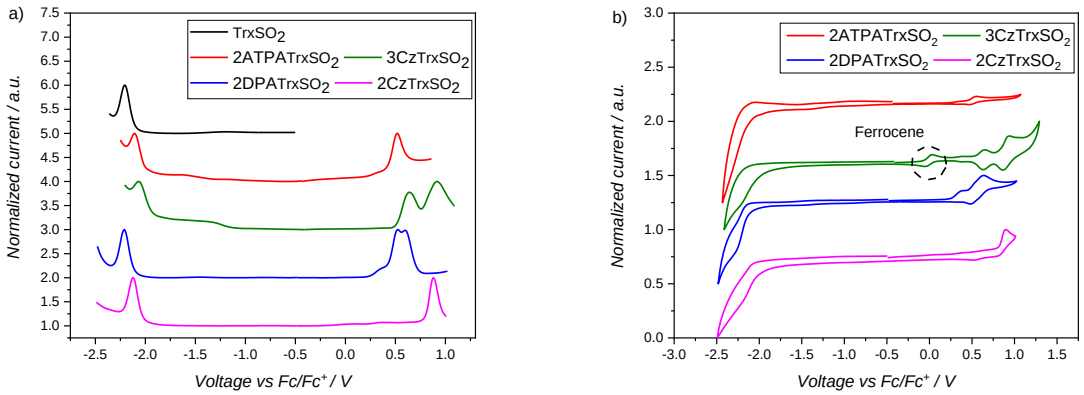

Figure 3. [a)]Square-wave voltammetry (SWV) traces and [b)]cyclic voltammograms (CV) of the $TrxSO_2$ derivatives and $TrxSO_2$ as a comparison in DCM solution with 0.3 M [TBA][PF_6] as the supporting electrolyte and Fc/Fc^+ as the internal reference.

Table 4. Electrochemical properties.

Emitter	E^{ox} [a)] [V]	E^{red} [a)] [V]	HOMO[b)] [eV]	LUMO[b)] [eV]	ΔE[c)] [eV]
$2DPATrxSO_2$	0.52	-2.21	-5.32	-2.59	2.73
$2ATPATrxSO_2$	0.51	-2.11	-5.31	-2.69	2.62
$2CzTrxSO_2$	0.88	-2.12	-5.68	-2.68	3.00
$3CzTrxSO_2$	0.64	-2.07	-5.44	-2.73	2.71
$TrxSO_2$	-	-2.21	-	-	-

[a)]Measured in DCM with 0.3 M [nBu$_4$N]BF_4 as the supporting electrolyte and Fc/Fc^+ as the internal reference; [b)]The HOMO and LUMO energies were calculated using the relation $E_{HOMO/LUMO} = -(E^{ox}_{pa,1}/E^{red}_{pc,1} + 4.8)$eV, where E^{ox}_{pa} and E^{red}_{pc} are anodic and cathodic peak potentials, respectively; [c)]$\Delta E = -(E_{HOMO} - E_{LUMO})$.

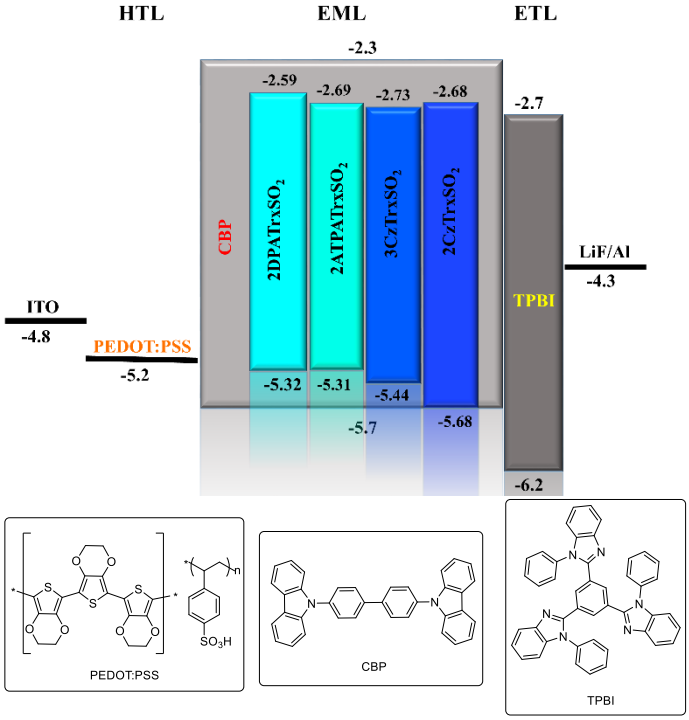

Figure 4. Schematic diagram of the devices with the energy levels and molecular structures of the organic compounds.

Table 5. EL performance of OLEDs.

Emitter	CIE[a] [x, y]	$EQE_{max/100/1000}$[b] [%]	$PE_{100/1000}$[c] [lm/W]	$CE_{100/1000}$[d] [cd/A]	$V_{100/1000}$[e] [V]	RO[f] [%]
$2DPATrxSO_2$	0.16, 0.34	10.6/5.5/3.6	4.5/2.3	11/7.4	7.7/10.3	66
$2ATPATrxSO_2$	0.22, 0.40	7.2/7.0/6.0	7.3/4.7	17/15	7.2/9.7	17
$2CzTrxSO_2$	0.17, 0.10	4.2/3.7/2.6	0.84/0.45	2.7/1.9	10.1/13.3	38
$3CzTrxSO_2$	0.16, 0.10	3.9/3.3/2.1	0.90/0.44	2.6/1.7	9.1/12.1	46

[a]Commission Internationale de l'Eclairage 1931 coordinates; [b]external quantum efficiency; [c]power efficiency; [d]current efficiency; [e]voltage; [f]EQE roll-off from maximum value to that at 1000 cd/m^2, determined by $(EQE_{max}-EQE_{1000})/EQE_{max}$.

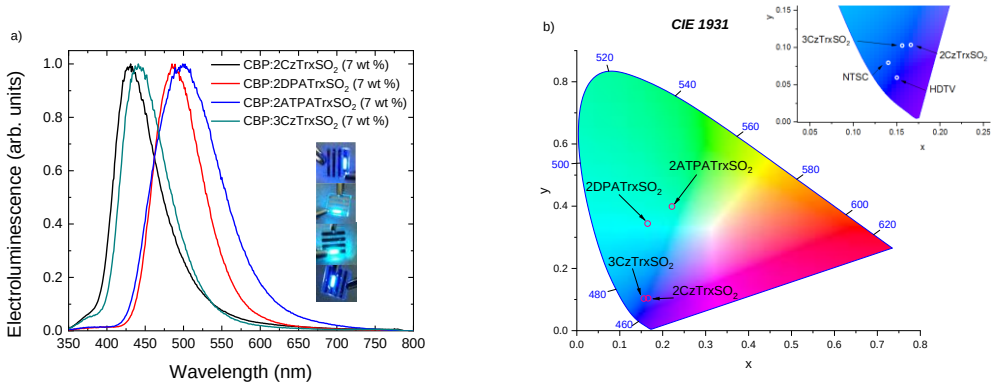

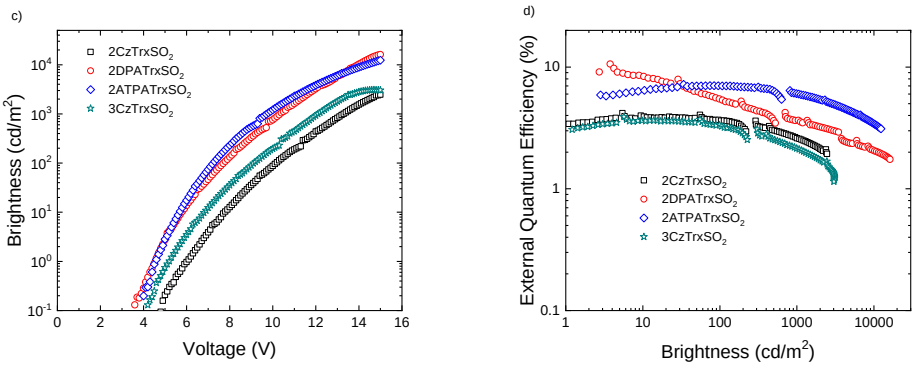

Figure 5. [a)]Electroluminescence spectra; [b)]CIE diagram with coordinates; [c)]Luminance-voltage; [d)]EQE-luminance curves of studied materials.

A new type of high-performance, good solubility and thermally-stable emitters based on novel unsymmetrical heterotruxene core, functionalized with carbazole and diphenylamine are introduced. The EL efficiencies of solution processed devices reach 3.7 % for deep blue emitter and 7.0 % for green emitter with C.I.E. color co-ordinates (0.16, 0.09) and (0.22, 0.40), respectively at 100 cd/m^2.

Keyword organic light-emitting diodes (OLEDs).

M. R. Maciejczyk,* S. Zhang, G. J. Hedley, N. Robertson,* I. D. W. Samuel,* and M. Pietraszkiewicz

Monothiatruxene based solution-processed green, sky-blue and deep-blue organic light-emitting diodes with efficiencies beyond 5% limit

ToC figure